

Microstructure and Rheology of Soft to Rigid Shear-Thickening Colloidal Suspensions

Safa Jamali and Arman Boromand

*Department of Macromolecular Science and Engineering, Case Western Reserve University,
Cleveland, OH 44106*

Norman Wagner

*Department of Chemical and Biomolecular Engineering, Center for Molecular Engineering and
Thermodynamics, University of Delaware, Newark, Delaware 19716*

Joao Maia

*Department of Macromolecular Science and Engineering, Case Western Reserve University,
Cleveland, OH 44106*

Synopsis

The shear rate-dependent rheological properties of soft to rigid colloidal suspensions are studied using computational models. We show that a contact force defined based on an elasto-hydrodynamic deformation theory captures an important rheological behavior of colloidal suspensions: While near hard-sphere particles exhibit a strong and continuous shear-thickening regime at high Péclet numbers when the hydrodynamic stresses become larger than the modulus of the colloidal particles. We measure N_1 and N_2 to be large and negative in the shear-thickening regime; however, for soft spheres at the onset of second shear-thinning N_2 reduces in magnitude and eventually becomes positive. We show that for near hard-sphere suspensions, colloidal

pressure, shear stress, and normal stress difference coefficients tend to diverge near the maximum packing fraction while $P > \sigma > N_1 > N_2$.

1. Introduction

The non-Newtonian rheological response of colloidal suspensions in different flow regimes is perhaps one of the most discussed, and yet controversial subjects in the field of fluid dynamics and physics. Of significant interest is the existence of shear thickening at high shear rates [Barnes (1989), Laun *et al.* (1992), Wagner and Brady (2009)] and this transition and its relationship to the rheology of non-Brownian suspensions is an ongoing discussion in the soft matter physics and rheology communities [see for example Brown and Jaeger (2014), Mari *et al.* (2014), Gurnon and Wagner (2015)]. This is in part motivated by applications [Lee *et al.* (2003)]. Regardless of the differences in the details of models and theories suggested to explain the rate-dependent rheology of suspensions, there is a consensus that as these macroscopic measures change under different flow conditions, the microstructure of the suspension undergoes transitions/changes correlatively [Mewis and Wagner (2012)].

Recent advances in the experimental capabilities, such as fast confocal microscopy [Cheng *et al.* (2011)] and neutron scattering measurements [Gurnon and Wagner (2015)] of the sheared suspensions have brought new insight into the microstructural state of a suspension under different flow regimes. At the same time, accurate measurements of the rheological properties were made possible by advanced normal stress transducers and controlled stress rheometry, enabling reliable rheological characterization of the suspensions [Cwalina and Wagner (2014)]. Computational studies have also contributed significantly to the current understanding of the microstructure-rheology relationship in colloidal suspensions. Recently, a series of simulations

and theoretical reports [Fernandez *et al.* (2013); Seto *et al.* (2013); Mari *et al.* (2014)] based on frictional contacts have successfully reproduced the so-called Discontinuous Shear-Thickening (DST), with remarkable agreement compared to experimental results. On the other hand, the notions of hydrocluster formation and lubrication driven shear-thickening at high shear rates have been able to reproduce the proper microstructure and rheological properties with semi-quantitative success compared to experimental measurements [D'Haene *et al.* (1993); Bender and Wagner (1996); Foss and Brady (2000); Kalman and Wagner (2009); Morris (2009); Jamali *et al.* (2013); Gurnon and Wagner (2015)]. In the following, we briefly discuss the various theories and some of the experimental studies on the rheological characterization and material properties of a colloidal suspension in the shear-thickened state.

At equilibrium at rest, stable, hard-sphere like colloidal dispersions can exist as a liquid and thus, the microstructure of the suspension is isotropic. The total force on a colloid is dominated by the Brownian motion, excluded volume and any other colloidal forces. As the suspension is subject to shear flows, the microstructure and the rheological response changes. At low and intermediate shear rates, Brownian forces are not sufficiently strong to compete with the external forces, and the microstructure becomes anisotropic and the suspension shear-thins. At these shear rates the particles tend to follow each other's path in the flow direction, which reduces the rate of energy dissipation during flow. At the macroscopic scale this results in shear-thinning of the suspension, as the Brownian contribution to the stress does not grow in proportion to the external forces driving the higher shear rates. This continues to the point where the average distance between the colloidal particles is small enough for the hydrodynamic interactions to dominate via lubrication stresses. Since the lubrication potential strictly depends on the surface separation distance of two interacting colloids, this effect is more pronounced for dense suspensions. At high shear rates,

the external shear forces reduce the average distance between the colloidal particles. Since the lubrication forces are of dissipative nature and retard the relative motion of particles, as the particles get in close proximity interacting colloids become localized in small gaps forming larger so-called hydroclusters [Maranzano and Wagner (2001)]. These hydroclusters resist the flow and give rise to shear-thickening behavior (for a summary of shear-thickening, see Bergenholz *et al.* (2002) and Wagner and Brady (2009)). At these shear rates, the net force on a colloidal particle and consequently the microstructure as well as the rheological response of a suspension is dictated by the hydrodynamic interactions. Since this versatile rate-dependent response of a suspension is governed by the competition between the hydrodynamic and Brownian forces, these distinct regimes are frequently presented as a function of a dimensionless

quantity, the Péclet number, $Pe = \frac{6\pi\eta_0\dot{\gamma}R^2}{k_B T/R}$. In this, the shear rate-dependent numerator

represents the strength of the hydrodynamic forces and the Brownian forces are represented in the denominator.

Recently, several studies have revisited the theory of dilatancy and frictional contacts in non-Colloidal suspensions [Fernandez *et al.* (2013); Heussinger (2013); Seto *et al.* (2013); Brown and Jaeger (2014); Wyart and Cates (2014)]. The reports suggest that at very small separation distances, the lubrication layer breaks down and contact between the two particles occurs. As soon as this contact point is formed, the microstructure and the motion of the suspension is governed by the competition between the normal repulsive contact potentials and the tangential friction forces. Thus, a stick-slip mechanism based on the Amundsen's law of friction is adapted to explain the frustrated motion of colloidal particles. Frustrated motion of colloidal particles is referred to a state where due to high packing of solid particles and high friction coefficient,

colloidal particles are constantly rotated in opposing directions. In several reports based on this methodology, DST and S-shaped stress curves for suspensions were reproduced successfully by tuning the friction coefficient of the particles. It is unknown if this phenomena extends to colloidal dispersions where surface stabilization leads to very low friction coefficients [Gurnon and Wagner (2015)].

While viscosity is perhaps the most indicative rheological fingerprint of a suspension's microstructure, drawing a comprehensive picture of the micro-macro relationship is only possible by considering the complete tensorial form of the stress, including the normal stresses. In other words, one can claim proper dynamics and the underlying physics only if the complete rheological characterization of a suspension is reproduced. In addition to the shear viscosity, the microstructural changes in a suspension under flow also affect the normal stresses. Under shear flow, the deviatoric stress tensor is characterized by the first and second normal stress differences, N_1 and N_2 , which are generally of smaller magnitudes as compared to shear stresses [Macosko (1994)]. Hence, the number of experimental reports where these two parameters are accurately measured for colloidal suspensions are very limited; however, recent advances in the rheometry techniques has allowed reliable measurements of normal stress differences for dense suspensions at high shear rates [Cwalina and Wagner (2014)]. In addition to the experimental evidence (which will be briefly discussed later), one can predict the microstructure and the normal stresses of a suspension in different regimes based on the theoretical approaches explained before. The hydrocluster formation as a result of large lubrication stresses suggests that the colloids will be concentrated in the compression axis of the shear plane [Foss and Brady (2000)]. Subsequently, particles will form a highly anisotropic structure where the probability of finding a neighboring colloid in a close vicinity is much larger than other coordinates. This

anisotropic microstructure leads to hydrodynamic contributions to the normal stress differences that are negative for both N_1 and N_2 . A detailed explanation of the effect of microstructure on the sign and magnitude of normal stress differences (based on the hydrodynamics theory) can be found in Foss and Brady (2000) and exact calculations for Brownian hard spheres can be found in Bergenholz *et al.* (2002). On the other hand, the frictional contact model is based on the competition between the tangential and normal forces. At high friction coefficients, the tangential forces dominate the type of interaction between the two overlapping colloids and their frustrated movement gives rise to an effective transient contact network to be formed at high shear rates. This contact network is able to bear large amounts of stresses and thus DST can be reproduced by this method. In other words, shear-thickening is recovered only at the conditions where the tangential friction dominates the net force on a single colloidal particle. Obviously, at these conditions one can expect positive N_1 and negative N_2 to be measured due to the nature of frictional forces [Mari *et al.* (2014)].

Several experimental studies have reported measurements of these properties. One should be cautious when referring to these data, as in many cases the authors state that the results are associated with intrinsic instrument limitations. The first quantitative measurements of normal stress differences were done by Laun (1994), who reported the N_1 of the same magnitude as the shear stress with a negative sign, and N_2 with half of this magnitude and a positive sign, for a 58.7 vol% suspensions of styrene/ethyl acrylate copolymer particles. Aral and Kalyon (1997) reported increasing negative first normal stresses differences by increasing the volume fraction of non-colloidal particles and the shear rate. Another example of the negative N_1 in the shear-thickening regime was reported by Lee *et al.* (2006) for near hard-sphere suspensions. Although experimental limitations prevented the authors from reporting quantitatively reliable second

normal stress differences, it was stated that the magnitude of N_2 is larger than the N_1 . Accurate normal stress measurements of colloidal suspensions were reported in a recent study by Cwalina and Wagner (2014), where negative normal stress differences were reported for a range of different volume fractions at the shear-thickening regime. N_1 and N_2 were found to be linearly increasing functions of shear rate in the shear-thickened state, which enabled the authors to define the shear-thickened state and consequently calculate the material properties such as first and second normal-stress different coefficients and the maximum packing fraction at the shear-thickened state.

Theoretically, at the very close distances between the colloidal particles and at high shear rates, where the shear stresses are extremely large, the particles start to deform elasto-hydrodynamically [Meeker *et al.* (2004)]. To explain this phenomenon, one has to take into account the fact that colloidal particles in real experiments have finite hardness or modulus, and thus will begin to deform as soon as the normal stresses exerted on them exceeds this modulus. Kalman [Kalman and Wagner (2009) and Mewis and Wagner (2012) (section 8.3.5)] showed that by taking this deformation into account one can semi-quantitatively explain the second shear-thinning regime, which is usually observed for soft suspensions [Hoffman (1972), Laun (1984), Barroso *et al.* (2010)]. Kawasaki *et al.* (2014) recently reported a series of Brownian Dynamics simulations on soft repulsive particles without hydrodynamic forces that reproduced shear rheology of soft latex dispersions and oil-water emulsions at high packing fractions. Nevertheless, the computational models to date have not been able to precisely study and examine the elasto-hydrodynamic theory. This is because in numerical approaches, a hard short-ranged repulsive force is usually employed to define the hard-sphere identity of a colloidal particle. To explore the effects of particle hardness on suspension rheology, we present a

computational approach based on a modified Dissipative Particle Dynamics formalism that captures the deformability of a colloidal particle. By using this method, we study the microstructural changes of a suspension at different flow regimes that lead to the bulk rheological response. The model employs a simple squeezing mode lubrication hydrodynamics and neglects other modes of hydrodynamics such as tangential lubrication, as well as frictional contacts. Consequently, continuous shear-thickening is reproduced and studied as opposed to discontinuous shear-thickening and dilatancy which may require inclusion of frictional contacts and tangential forces.

2. Simulation Background

Dissipative Particle Dynamics (DPD) was introduced initially [Hoogerbrugge and Koelman (1992)] for simulation of colloidal suspensions under flow conditions. The explicit solution of the equation of motion for solvent particles, and a built-in thermostat that forms the canonical ensemble, and a series of pairwise interactions that ensure conservation of momentum in a system, enables the long range hydrodynamics to be naturally preserved in the DPD formalism. However, the early attempts on shear rheology of suspensions using DPD had a limited success as the hydrodynamics breaks down at the close separation distances [Whittle and Dickinson (2001)]. As the distance between two interacting colloidal particle becomes smaller than the size of a solvent particle, when these colloids move towards each other the solvent is expelled from in between the two, and thus the hydrodynamics breaks down. Another reason for the shortcoming of DPD in simulation of sheared suspensions is the size/mass differences between the solvent and colloidal particles. In traditional DPD, all particles regardless of their type have the same size and mass. Consequently, to reproduce a realistic suspension where colloidal particles are many times larger than the solvents, many DPD particles are linked to each other to form a larger

aggregate to represent a single colloid. However, in this process, the smooth definition of the colloidal surface is lost and calculation of forces that are strictly dependent of the surface-surface separation distances becomes problematic. In our modified DPD model, inspired by the model proposed by Whittle and Travis (2010), we use an arbitrary-sized rigid core to represent the colloidal particle, with additional lubrication potentials to compensate for the short-ranges lubrication interactions. Thus, the equation of motion for a colloidal particle in this formalism is written based on 5 main pairwise interaction potentials.

$$m_i \frac{d\mathbf{v}_i}{dt} = \sum \mathbf{F}_{ij}^C + \mathbf{F}_{ij}^D + \mathbf{F}_{ij}^R + \mathbf{F}_{ij}^H + \mathbf{F}_{ij}^{Contact} \quad (1)$$

This equation reduces to the first 3 forces for the solvent particles, where only conservative, random and dissipative interactions are solved. The first force, conservative, is the extent of pressure between the interacting species and for the solvents is parametrized based on the compressibility of water at ambient temperature, $a_{ij} \approx k_B T \frac{\kappa^{-1} - 1}{0.2\rho}$ [Groot and Warren (1997)], where ρ is the number density of DPD particles. Equation 2 shows the expression for the conservative force, where a_{ij} is the conservative parameter, $\omega_{ij}(r_{ij})$ is the weight function based on the separation distance between the interacting particle pair, and \mathbf{e}_{ij} is the unit vector as

$$\mathbf{e}_{ij} = \frac{\mathbf{r}_{ij}}{|\mathbf{r}_{ij}|}.$$

$$\mathbf{F}_{ij}^C = a_{ij} \omega_{ij}^C(\mathbf{r}_{ij}) \mathbf{e}_{ij} \quad (2)$$

The random force generates the thermal fluctuations in the system using a random function, Θ_{ij} ,

of zero mean value and unit variance. Δt in equation 2 is the time step used in the simulation, and σ_{ij} is the strength of the thermal fluctuations in the system.

$$\mathbf{F}_{ij}^R = \sigma_{ij} \omega_{ij}^R(\mathbf{r}_{ij}) \frac{\Theta_{ij}}{\sqrt{\Delta t}} \mathbf{e}_{ij}, \quad (3)$$

The dissipative force acts against the relative velocity of particles, $\mathbf{v}_{ij} = \mathbf{v}_i - \mathbf{v}_j$ as the heat sink and dissipates the generated heat in the random force and ensures the proper thermodynamics to be reproduced. Hence, the dissipative parameter (frequently referred as friction parameter), γ_{ij} has to be coupled to the random parameter in equation 3 [Espanol and Warren (1995)]. This is done via the so-called fluctuation-dissipation theorem and consequently the dimensionless

temperature in the system is defined as $\frac{\sigma_{ij}^2}{2\gamma_{ij}} = k_B T$. Additionally, the weight functions used in

these forces are inter-related via the equation 5. In fact, all of the DPD potentials are calculated via this weight function which starts at unity and decays to zero at a distance called the cut off. In the standard DPD method, the interparticle potentials are so soft that often the cut off distance is assumed as the diameter of a DPD particle, as the particles are allowed to overlap and pass through one another.

$$\mathbf{F}_{ij}^D = -\gamma_{ij} \omega_{ij}^D(\mathbf{r}_{ij}) (\mathbf{v}_{ij} \cdot \mathbf{e}_{ij}) \mathbf{e}_{ij}, \quad (4)$$

$$\omega_{ij}^C(\mathbf{r}_{ij}) = \omega_{ij}^R(\mathbf{r}_{ij}) = [\omega_{ij}^D(\mathbf{r}_{ij})]^{0.5} = \omega_{ij}(\mathbf{r}_{ij}) = \begin{cases} \left(1 - \frac{r_{ij}}{r_c}\right); & r_{ij} \leq r_c \\ 0; & r_{ij} \geq r_c \end{cases} \quad (5)$$

One of the hallmarks of DPD is that although the random force is the main source of Brownian motion in a DPD fluid, since together with the dissipative force, they conserve the momentum both locally and globally, the two forces also preserve the proper long-range and multi-body hydrodynamics. In addition to these forces, which are used for solving the equation of motion for both solvent and the colloidal particles, the short-range lubrication potential, \mathbf{F}_{ij}^H , and the contact forces, $\mathbf{F}_{ij}^{Contact}$, are also introduced for the colloidal particles. The former is based on the pair drag term, μ_{ij}^H , in squeeze mode hydrodynamics [Ball and Melrose (1995)], which diverges at the surface-surface contact point, $h_{ij} = 0$ (equation 6). R is the radius of the colloidal particle and η_0 is the viscosity of the suspending fluid. Since the lubrication potential is singular at the contact, a small gap, δ , is introduced to the pair drag term to regularize this force. At these distances, the lubrication potential becomes independent of the surface-surface distance between the two interacting colloids.

$$\mathbf{F}_{ij}^H = -\mu_{ij}^H (\mathbf{v}_{ij} \cdot \mathbf{e}_{ij}) \mathbf{e}_{ij}; \mu_{ij}^H = \begin{cases} \left(\frac{3\pi\eta_0 R^2}{2\delta} \right), & 0 < h_{ij} \leq \delta \\ \left(\frac{3\pi\eta_0 R^2}{2h_{ij}} \right), & h_{ij} > \delta \end{cases}, \quad (6)$$

Silbert *et al.* (1999) showed that at high shear rate, the dominant mode of hydrodynamic interactions in dense suspensions is the squeezing mode lubrication in normal direction which diverges at contact with $\frac{1}{h_{ij}}$ where h_{ij} is the surface-surface separation distance between two colloidal particles. On the other hand, tangential lubrication potential is also singular at contact point, however it diverges with $\log(\frac{1}{h_{ij}})$. Thus, it has been shown that the normal lubrication

potentials are predominantly playing the main role in defining the hydrodynamic interactions at close gaps and neglecting the tangential lubrications does not significantly affect the behavior of the suspension.

The contact force, $\mathbf{F}_{ij}^{Contact}$, defines the rigid nature of the colloidal particles and prevents the overlap between the two cores, and vanishes cubically at a small separation distance, Δ , comparable to the roughness of the surface of a colloidal particle in real experiments. Additionally, since the real particles have finite modulus the softness and hardness of colloids can be adjusted by tuning the magnitude of the contact modulus, $f^{Contact}$.

$$\mathbf{F}_{ij}^{Contact} = \begin{cases} f^{Contact}(1+h_{ij}), & h_{ij} \leq 0 \\ f^{Contact}\left(1-\frac{h_{ij}}{\Delta}\right)^3, & 0 < h_{ij} \leq \Delta \\ 0, & h_{ij} > \Delta \end{cases} \quad (7)$$

Based on the definition of the contact potential, which only acts on distances comparable to the surface roughness of a colloidal particle, one can assume Δ to be in the range of 1 nm. On the other hand DPD parameters can be systematically correlated to the real units, adapting the method proposed by Ghoufi and Malfreyt (2012). By doing so, the correspondence of contact

modulus to real units is $f^{Contact} \frac{k_B T}{\Delta^3}$, where k_B is the Boltzmann constant, and T is ambient temperature in Kelvin. Thus, shear moduli of 400 MPa and 100 GPa corresponding to $f^{Contact}$ of the softest (100) and the most rigid (25000) particles in our simulations. Consequently, shear moduli of real particles reported by Kalman (2010) are estimated to be $f^{Contact} \approx 250$ for PMMA particles (1 GPa) and $f^{Contact} \approx 11000$ for Silica particles (44 GPa).

In our methodology we assume elasto-hydrodynamic deformation of colloidal particles at close gaps. In other words, instead of assuming a contact that breaks the lubrication layer and allows particles to stick to one another, we assume that as the particles get closer to each other the hydrodynamic stresses continue to increase and eventually will elastically deform the particles. Thus, in the event of overlap between the colloidal cores, the contact force increases linearly. It has been previously shown that the stress level between the particles at this condition, depends directly on the value of the shear modulus of colloids [Kalman (2010), Mewis and Wagner (2012) section 8.3.5]. This is in contrary to the model adapted in recently developed frictional contact models [Seto *et al.* (2013)], where a stick-slip scenario is considered based on the frictional contact models of granular physics. In our model, the contact forces are only applied in the normal direction and tangential forces are neglected (both in contacts and the lubrication).

Having the individual pairwise interactions at hand, one can calculate the pressure/stress tensor by the Irving and Kirkwood (1950) method, and consequently measure the rheological properties such as the shear viscosity from the shear component of the stress tensor as $\eta = \frac{\langle S_{12} \rangle}{\gamma}$, and the first and second normal stress differences as $N_i = S_{ii} - S_{(i+1)(i+1)}$.

$$\mathbf{P} = \frac{1}{V} \left\{ \sum_{i=1}^N m_i (\mathbf{v}_i - \mathbf{u}(r_i)) \otimes (\mathbf{v}_i - \mathbf{u}(r_i)) + \sum_{j>i} \sum_{i=1}^{N-1} \mathbf{r}_{ij} \otimes \mathbf{F}_{ij} \right\}, \quad (8)$$

In practice, we have performed simulations on suspensions with different volume fractions of the total number density of 3.0 and dimensionless temperature of $k_B T = 1.0$ in the calculation box of $L_{i=x,y,z} = 25R$. Colloidal particles with $R = 1.0$ were reproduced with the mass of $m = \frac{4}{3} \rho \pi R^3$ in order to ensure the density matching between the solvent and the colloidal particles. It should be

mentioned that in order to avoid strong ordering under shear known to be present for monodisperse suspensions, a volumetric ratio of 1:1 of larger colloidal particles with $R=1.4$ were added to the mixture. The dissipative parameter was set at $\gamma_{ij}=50.0$ and correspondingly giving the random parameter of $\sigma_{ij}=10.0$, with conservative parameter of $a_{ij}=25.0$ for all interacting species. The clearance gap used for the regularization of the lubrication potential was set at $\delta=10^{-6}R$ and the surface roughness of the colloidal particles at which the contact potential is neutralized is set to $\Delta=10^{-3}R$ in order to reproduce the most realistic representation of a colloid. Although the contact force prevents overlap between the rigid cores of interacting colloids to occur, since finite time steps are used in discrete particulate simulation method, the event of overlap cannot be completely avoided. However, in order to reduce these events and the numerical instabilities in the calculations very small time steps of $\Delta t=5\times10^{-6}r_c\sqrt{\frac{m}{k_B T}}$ were used in our simulations. All of the simulations were performed over 10 million time steps to ensure steady and stable statistical results. The contact modulus was varied over a wide range to reproduce soft to rigid colloidal particles with $f^{Contact}=100-25000$.

3. Results and Discussion

3.1. Flow Curve

The general flow curve for suspensions with different volume fractions is shown in Figure 1, where each point represents a steady state. The suspensions show a general shear-thinning followed by shear-thickening at higher shear rates, regardless of the contact modulus and the volume fraction. At low volume fractions, the viscosity is nearly independent of the contact modulus and all suspensions exhibit the expected shear-thinning and weak shear-thickening;

however, differences arise for the denser suspensions with small values of contact modulus, where a second shear-thinning regime is observed at elevated Péclet numbers. This behavior is not observed for rigid particles. The onset of second shear-thinning is observed when the total stress exceeds the contact modulus of colloidal particles. In other words, the hydrodynamic stresses that give rise to shear-thickening of the suspension at high shear rates continue to increase to a point where they eventually become comparable to the elastic modulus of the colloidal particles. At this state, the hydrodynamic stresses begin to elastically deform the soft colloids, leading to shear thinning [Kalman and Wagner (2009), Mewis and Wagner (2012) section 8.3.5], while near hard-sphere particles only exhibit shear-thickening that becomes more pronounced with increasing shear rate.

Finally a graph is presented with the relative viscosity of the most rigid particles ($f^{Contact} = 25000$) for different fraction of solid particles compared to experimental measurements of Cwalina and Wagner (2014) and Stokesian Dynamics simulations of Foss and Brady (2000). The present model shows a comparable viscosity to the more accurate Stokesian Dynamics simulations in the low to moderate Pe number regime, but a stronger shear thickening than SD that is more comparable to experiment.

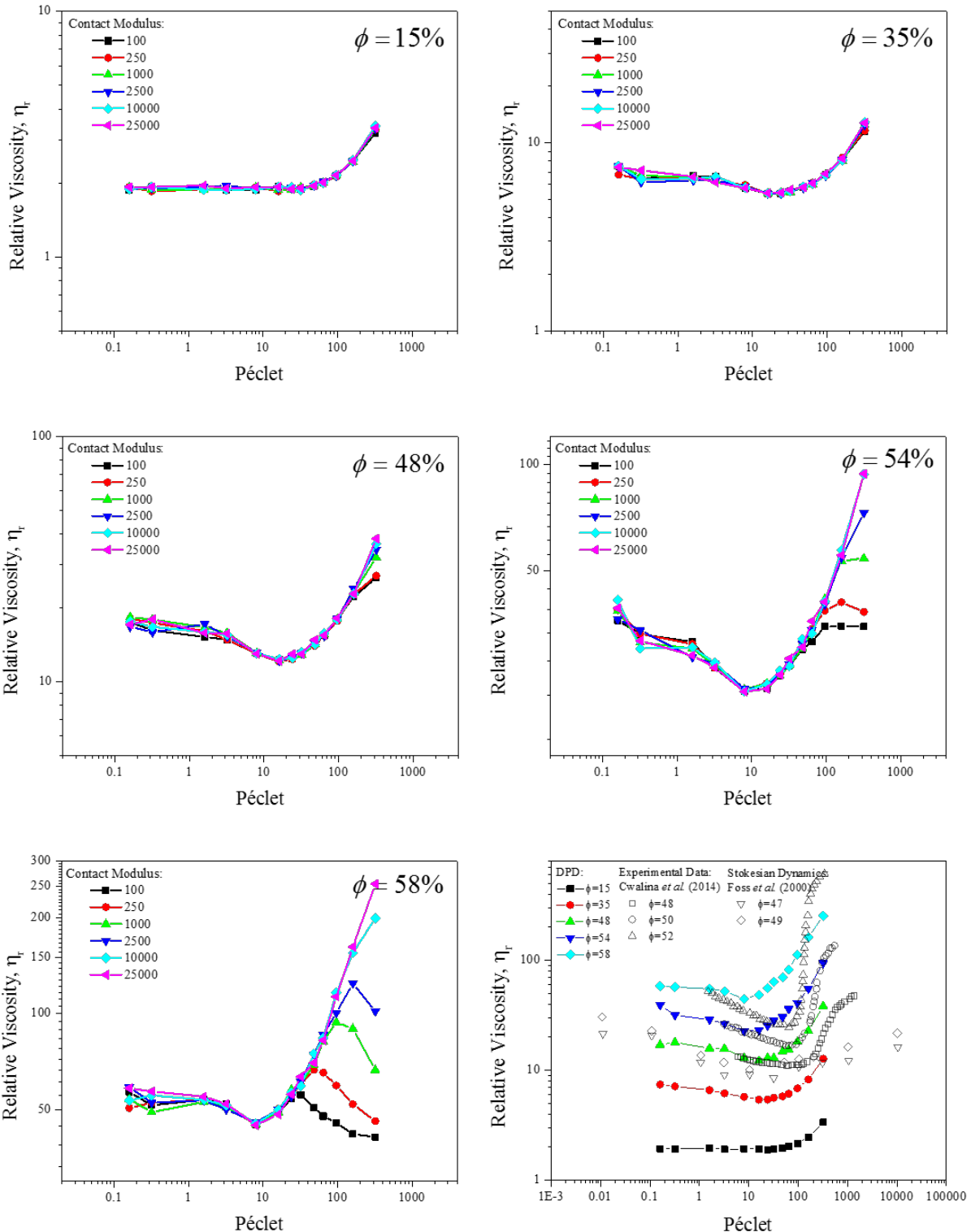


Figure 1. Viscosity vs. Péclet for different volume fractions and contact moduli. The bottom right graph compares the present work (contact modulus of 25000) with the experimental data by Cwalina and Wagner (2014) and Stokesian Dynamics simulations by Foss and Brady (2000).

Figure 2 shows the relative viscosity of the suspensions, $\eta_r = \frac{\sigma}{\eta_0 \dot{\gamma}}$, for different shear rates as a function of colloidal volume fraction and the results clearly show the difference between the soft and rigid particles. At low and intermediate shear rates, the viscosity v. volume fraction of colloidal particles curves is very similar for the soft and rigid suspensions; however, by increasing the shear rate the behavior of the dense regime is significantly different. Based on the empirical models to fit the viscosity curves in the figure 2 one can calculate the maximum packing fraction of each system at different shear rates.

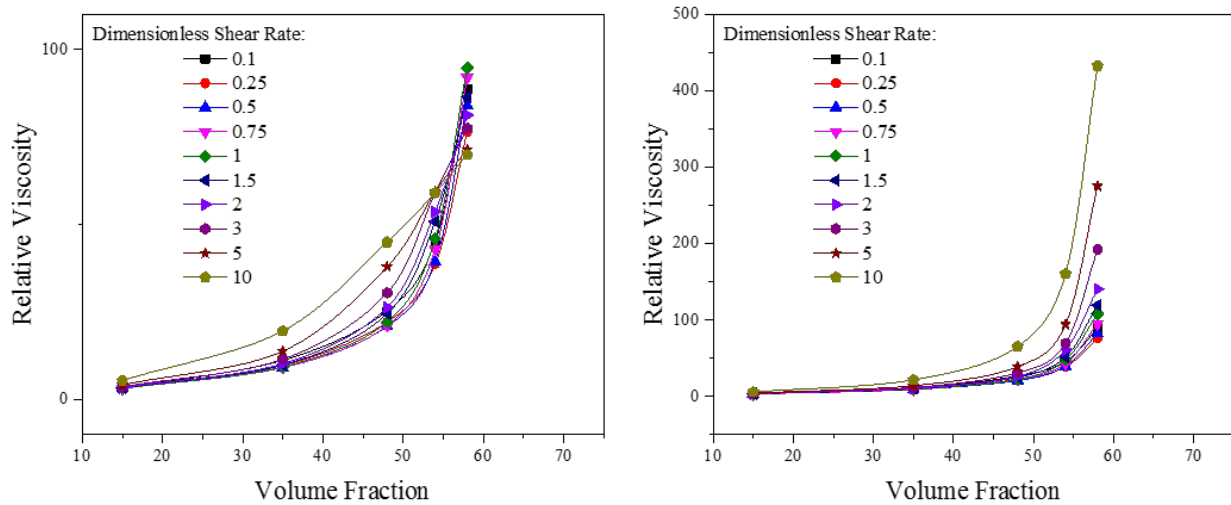


Figure 2. Relative viscosity against fraction of colloidal particles for: left) Soft colloid with modulus of 100, and Right) Rigid colloids of the modulus 25000.

Figure 3 shows the maximum packing fractions calculated based on two different models of Maron and Pierce (1956) (equation 9) and Eilers (1941) (equation 10):

$$\eta_r = \left(1 - \frac{\phi}{\phi_{Max}}\right)^{-2}, \quad (9)$$

$$\eta_r = \left[1 + 1.5\phi \left(1 - \frac{\phi}{\phi_{Max}} \right)^{-1} \right]^2, \quad (10)$$

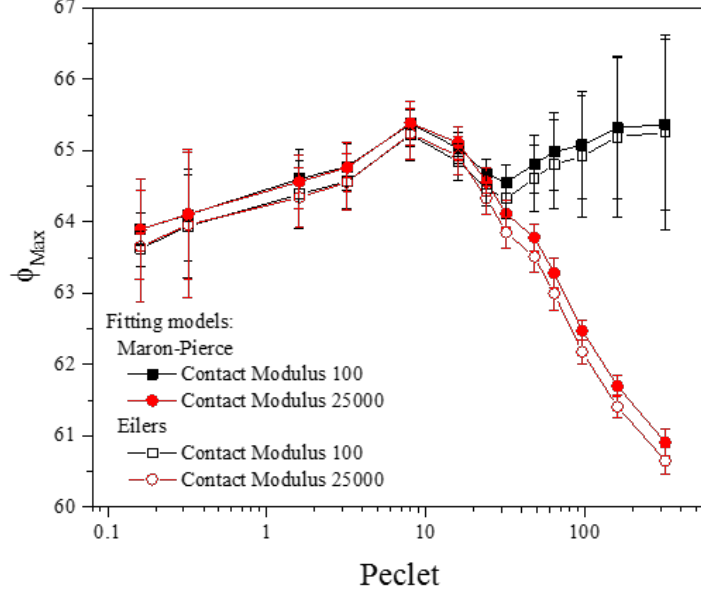


Figure 3. Maximum packing fraction calculated by different models versus the Péclet number for soft and rigid suspensions.

The expressions given in equation 9 and 10 are the empirical models that are often used to correlate experimental measurements of non-Brownian suspensions. Since at high shear rates, Brownian contribution to the viscosity can be neglected for our colloidal systems, we employ the same equations to fit our viscosity data. As the results are not statistically different using these two functionally different equations, the important trends observed are deemed significant and not dependent on the choice of extrapolation model. One can clearly correlate the calculated maximum packing fractions in Figure 3 with the general flow curves in Figure 1. In the shear-thinning regime, the maximum packing slightly increases as the suspensions are dominated by the Brownian forces at zero shear rate and a maximum packing of ~0.57 is expected [Russel *et al.* (2013)] and progressively become dominated by hydrodynamic interactions with increasing shear rate [de Kruif *et al.* (1985)]. However, at the onset of shear-thickening, the maximum

packing starts to decrease as the viscosity is mainly driven by short-range lubrication in this regime. For the rigid particles that continue to thicken by increasing the shear rate, this maximum packing fraction is reduced steadily. This in agreement with findings of Cwalina and Wagner (2014), who calculated a constant maximum packing for the shear-thickened-state of suspensions, at lower fractions compared to the high shear maximum packing fractions for near hard-sphere particles. It should be mentioned that in our results there is no clear second plateau to define a clear shear-thickened state, which explains the continuously decreasing curve of ϕ_{Max} as opposed to a constant value at high Péclet numbers. On the other hand, the maximum packing of the soft suspensions starts to grow as the second shear-thinning regime is observed.

The properties of the soft to rigid suspensions can be further examined by comparing the relative viscosities of suspensions with different moduli at a constant shear rate. Thus, in Figure 4 we plot the relative viscosities at the highest Péclet number in our simulations, Pe=320, and the maximum packing fractions calculated from these curves using the Eilers model (equation 10) against the hardness of colloidal particles. Furthermore, we have examined the role of lubrication interactions by running the same simulations without the hydrodynamics force in the equation of motion. Thus, the open symbols in the relative viscosity curve (and throughout the paper) correspond to the simulations where short-ranged hydrodynamic interactions are not included in the simulations. The relative viscosity at high Péclet numbers (Figure 4) clearly reflects the effect of particle softness, and the maximum packing fraction is significantly decreased by increasing the modulus of the colloidal particles. Also, the viscosity of the suspensions without the lubrication interaction clearly shows that the rheological response at high shear rates are dominated by the lubrication forces.

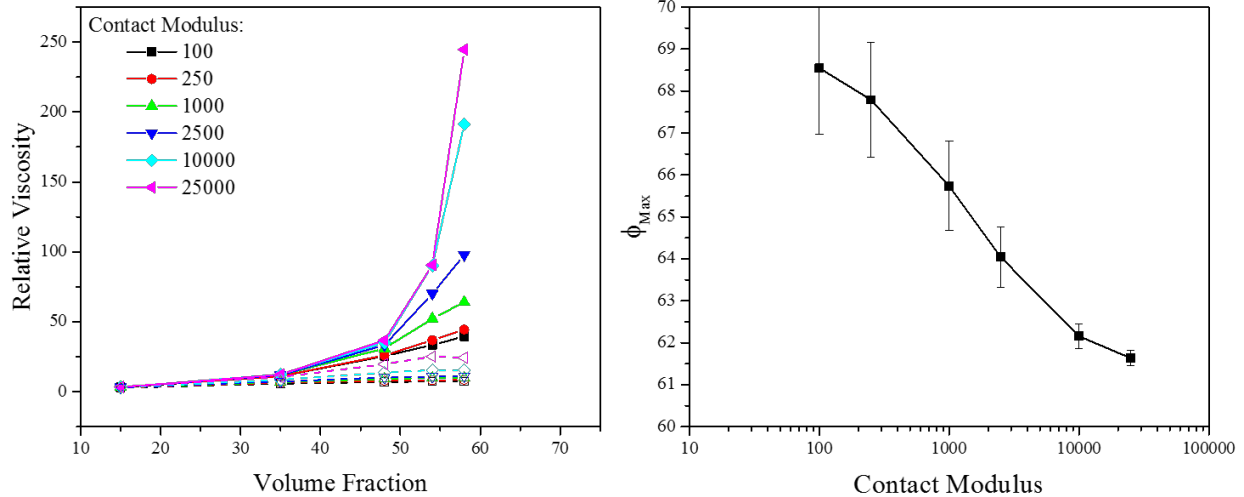


Figure 4. Left) Relative viscosity versus the colloidal fraction for a range of contact modulus values at high shear rate, $Pe=320$, and Right) Maximum packing fraction calculated from the relative viscosity as a function of modulus. Open symbols correspond to simulations without lubrication hydrodynamic interactions.

These findings are in agreement with the predictions of the elasto-hydrodynamic theory for the limiting viscosity of a suspension in the second shear-thinning regime. The elasto-hydrodynamic theory suggests that when the stresses exerted on a particle become sufficiently large, particles are elastically deformed. However, as the particles are made stiffer, a point is reached where the stresses generated in the suspension at a given shear rate are never large enough to overcome the rigidity of the particle and thus, the viscosity becomes independent of the particle rigidity. This is evident in Figure 4.right where a plateau is reached as the particle rigidity is increased further.

Based on the modulus of a colloidal particle, applied shear rate and the viscosity of suspending fluid one can predict the limiting viscosity of an elastically deforming suspension at high Peclet numbers [Kalman (2010); Mewis and Wagner (2012)]. According to this model, viscosity of a suspension is bound to the measured values in equation 11 in the elasto-hydrodynamic regime.

$$\eta_{EH} = C_{EH} \dot{\gamma}^{-\frac{1}{2}} (\eta_0 G_0)^{\frac{1}{2}}, \quad (11)$$

Where η_{EH} is the limiting viscosity in the elasto-hydrodynamic regime, C_{EH} is the prefactor depending on the volume fraction and the microstructure of the suspension and G_0 is the shear modulus of colloidal particles. The model predicts a second thinning regime and a positive dependence on the elasticity of the colloidal particles with scaling of $\frac{1}{2}$. Figure 5 shows the predictions of elasto-hydrodynamic model for measured viscosities in 58% suspensions of different moduli. The expression given in equation 11 for the limiting viscosity is based on the elasto-hydrodynamic stresses generated in the system and do not include the hydrodynamic stresses. Our softest colloid enters the elasto-hydrodynamic regime at lowest stress values and thus it is safe to assume that the stresses measured in these conditions are virtually hydrodynamic in nature. Hence by subtracting the viscosity of the softest system from the others, one can presumably track the changes in elasto-hydrodynamic viscosity. Thus assuming that the high Peclet limit viscosity of the softest suspension gives a pure hydrodynamic contribution to the stress, we have plotted the viscosity data after subtracting the value of the viscosity at the highest shear rate for the modulus of 100. Results of the figure 5 shows that not only the model can successfully predict the limiting viscosities at high shear rates, but also the viscosity of suspensions in the elasto-hydrodynamic regime scales with the modulus of colloidal particles with predicted power of $\frac{1}{2}$.

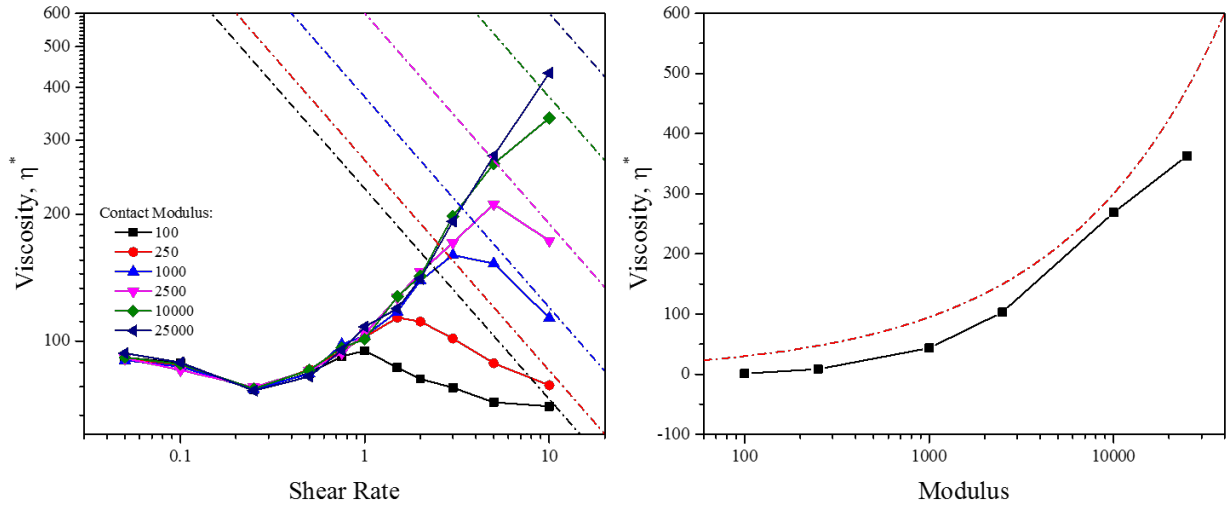


Figure 5. Reduced viscosity (subtracted by its value for suspension with modulus of 100 at shear rate of 10) of 58% suspensions as a function of: Left) Dimensionless shear rate and, Right) Particle modulus at shear rate of 10. Dashed lines represent the predictions of elasto-hydrodynamic model (equation 11).

3.2. Normal Stress Differences and Pressure

As discussed in the introduction, a complete rheological analysis including the normal stress measurements is crucial for understanding the underlying mechanisms. Thus, Figure 6 shows the measured N_1 and N_2 values for a range of volume fractions and contact modulus values. There are several observations to be made from the first and second normal stress difference measurements in Figure 6. Firstly, N_1 stays negative throughout the whole range of Péclet numbers regardless of the volume fraction and contact modulus of the colloidal particles. The only exception for this is at very low shear rates, where positive values are measured but remain negligible when compared to the total pressure of the system. At high shear rates and in the shear-thickening regime N_1 increases linearly with the Péclet number (shear rate), as observed by Cwalina and Wagner (2014). The second normal stress differences is also negative in the range of Péclet numbers examined; however, there is a clear change of behavior for soft and rigid colloidal particles at high shear rates. As the second shear-thinning occurs for the soft

suspensions, the magnitude of N_2 begins to decrease and eventually the sign of N_2 reverses to positive values at very high shear rates for the soft colloids. The magnitude of both quantities, $|N_1|$ and $|N_2|$, increases by increasing the particle volume fraction. Also one can argue that while at low volume fractions first normal stresses are substantially larger than the second normal stress differences, then $|N_2|$ increases faster by increasing the volume fraction and eventually becomes larger than the $|N_1|$ at elevated fractions. Another important conclusion from the Figure 6 is that, regardless of the colloidal fraction or the contact modulus, $|N_1|$ and $|N_2|$ remain small and independent of these parameters when lubrication potentials are excluded in the simulation, which confirms that hydrodynamic interactions dominate the rheological properties at these shear rates. In order to compare these results with prior reports on the near hard-sphere suspensions we plotted the N_1 and N_2 versus the shear stress in Figure 7 for the highest modulus in our simulations, $f^{Contact} = 25000$.

One can define the first and second normal stress coefficients for suspensions based on the shear stress of the suspending fluid and the measured N_1 and N_2 :

$$\Upsilon_{1,2} = \frac{-N_{1,2}}{\eta_0 \dot{\gamma}}, \quad (11)$$

The first and second normal stress difference coefficients for near hard-sphere colloids, Υ_1 and Υ_2 , show the same dependencies on the volume fraction of the solid content as the relative viscosity of the suspensions given in Figure 2. However, since N_2 exhibits an unexpected change of magnitude for the soft suspensions in the second shear-thinning regime, the typical divergence near the maximum packing fraction is not observed for Υ_2 of soft suspensions. In order to show

this behavior, we have plotted the first and second normal stress difference coefficients of the suspensions with different modulus values, at the highest shear rate examined in our simulations (Figure 8). One should note that as the contact modulus is increased, this data reveals the material properties for suspensions in the second shear-thinning (soft) to strong shear-thickening (hard) regime. Once again, we have plotted the same data for the simulations without the lubrication interactions, and represented the results with open symbols.

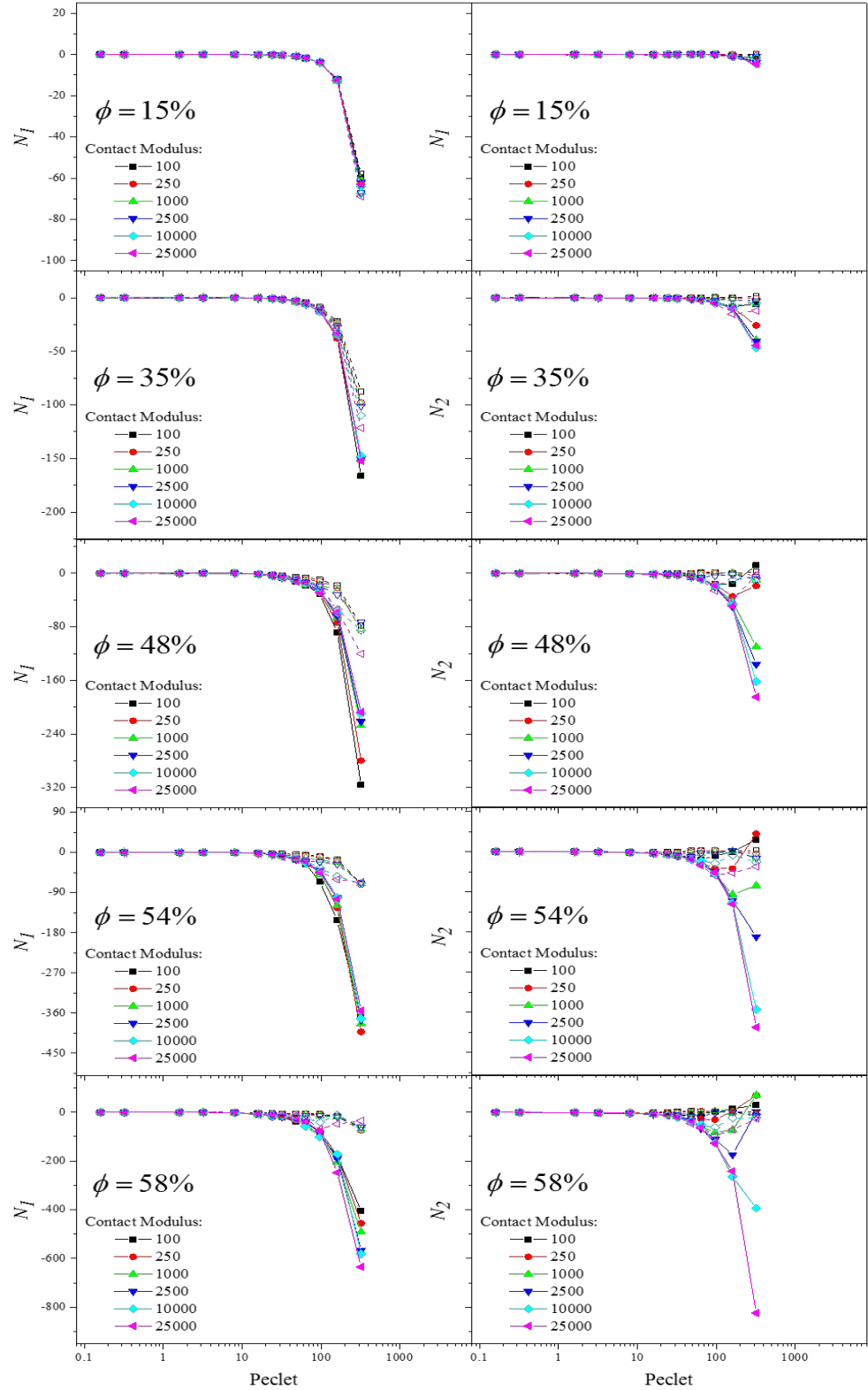


Figure 6. First (left) and second (right) normal stress differences versus the Péclet number for a range of volume fractions and contact modulus values. Open symbols correspond to simulations without lubrication hydrodynamics.

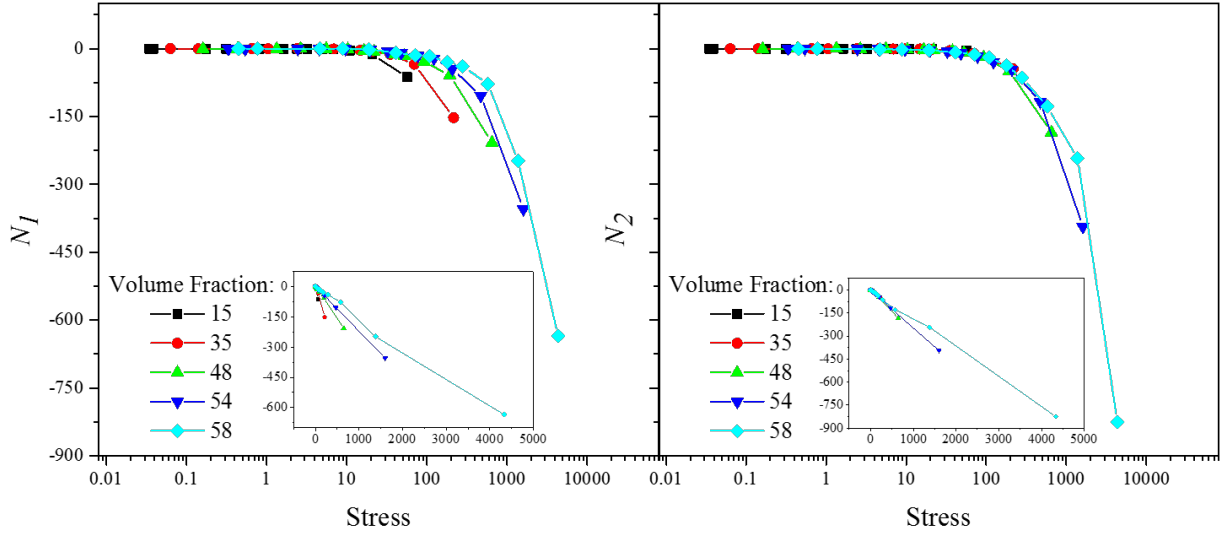


Figure 7. First (left) and second (right) normal stress differences versus the shear stress for different volume fractions of near hard-sphere suspensions (contact modulus of 25000). The insets show the data on a linear scale.

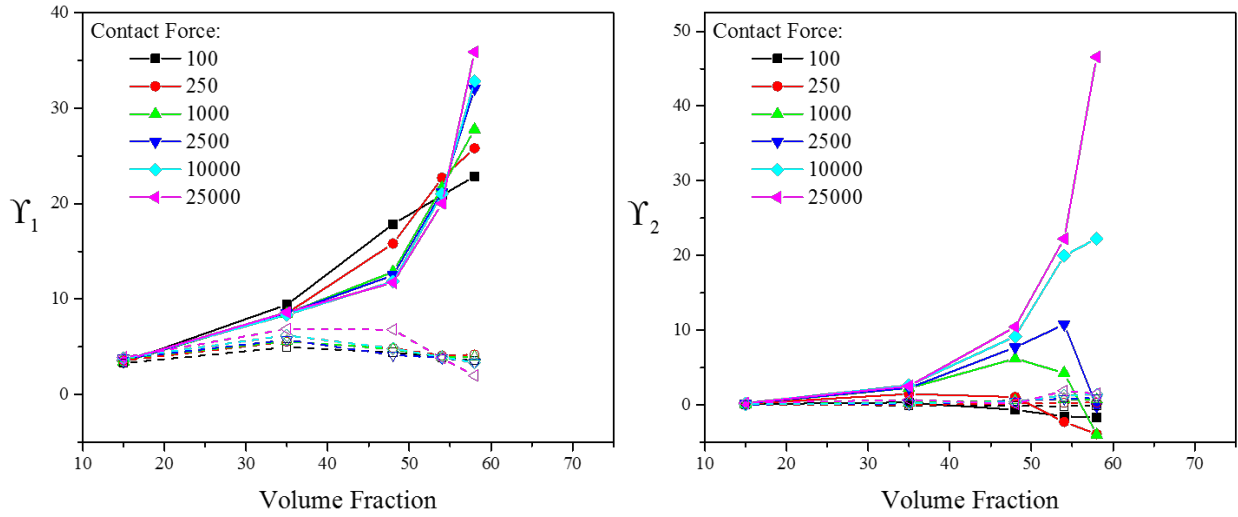


Figure 8. First (left) and second (right) normal stress difference coefficients versus the volume fraction of colloidal particles for a range of modulus values at highest shear rate ($Pe=320$). The open symbols are for simulations without hydrodynamic interactions.

Theoretically, the total pressure of the suspension should diverge near the maximum packing fraction, similarly to the relative viscosity and normal stress difference coefficients. The total pressure of the dense suspensions (58%) for different particle modulus values (Figure 9 left)

shows that while in the shear-thinning regime the pressure is rather unchanged, it begins to exponentially increase at the onset of shear-thickening. Nonetheless, in the case of soft particles pressure becomes constant in the second shear-thinning regime. The pressure at high shear rates ($\text{Pe}=320$) shows similar behavior when compared to the relative viscosities in Figure 4, as shown in Figure 9 right).

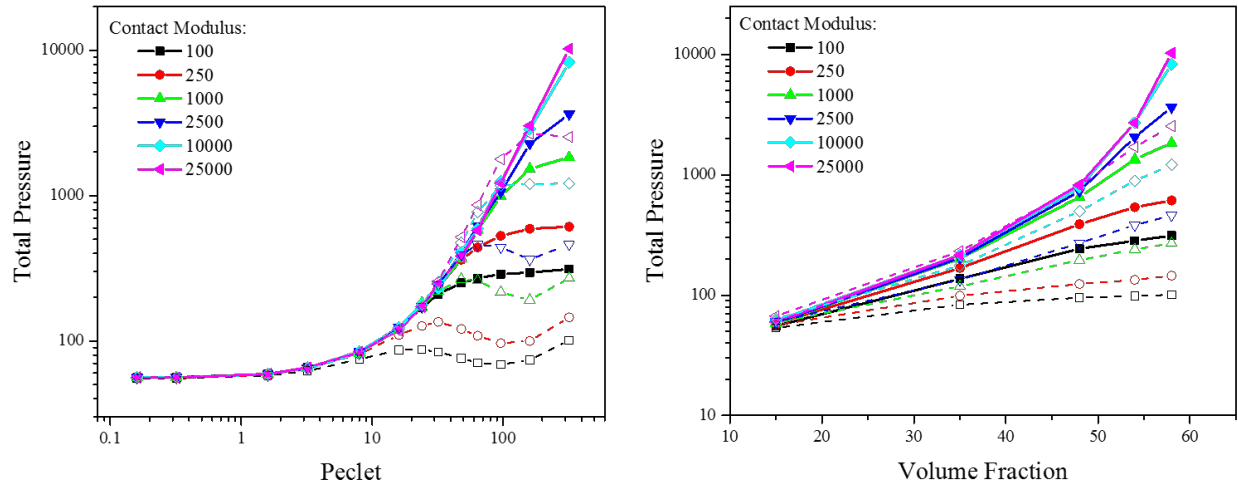


Figure 9. Total pressure of: Left) 58% suspensions versus the Péclet number, and Right) suspensions at $\text{Pe}=320$ vs. the solid particle volume fraction.

3.3. Microstructure

As noted in the introduction section, the rheological response of a suspension to different flow conditions is associated with changes in the microstructural configuration of colloidal particles. These microstructural changes are usually presented in the form of pair correlation function projected into specific planes of flow. The radial distribution function $g(r)$, is calculated in an isotropic fluid by calculating the probability of finding a neighboring particle at center-to-center distance r , i.e., the pair correlation function, without angular dependence. Pair correlation functions under flow become anisotropic and hence, angularly dependent. Here, the simulation box is divided into small layers (with sizes of less than the particle diameter) aligned in a specific

flow plane. Figure 10 plots the 2-D pair correlation functions of the soft (modulus of 100) and rigid (modulus of 25000) at different shear rates in the velocity-gradient plane. These structures show many features qualitatively similar to recent measurements, and even show evidence of four-fold symmetries as recently identified in shear thickening colloidal dispersions [Gurnon and Wagner (2015)].

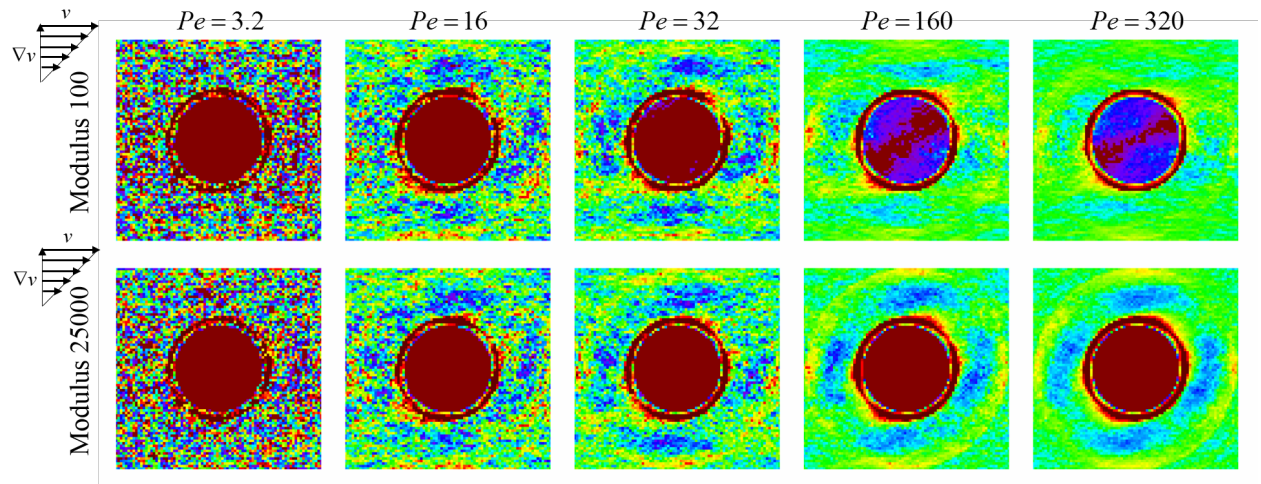


Figure 10. Pair correlation function in velocity-gradient direction for the softest and most rigid 58% suspensions over a range of shear rates.

The pair correlation functions in figure 10 show the different rheological regimes of each suspension. At the lowest Péclet number, both suspensions are in the shear-thinning regime where identical isotropic structures are observed. At the onset of shear-thickening, $Pe=16$, the microstructures start to show anisotropy, which continues to grow to be more evident at higher Péclet of 32. One can clearly observe similar microstructures for the soft and rigid suspensions in these regimes; however, at even higher shear rates, where the soft suspension exhibits a second thinning behavior, the pair correlation functions are significantly different. The rigid suspensions continue to form highly anisotropic structures where the colloidal particles are concentrated in the compressional axis. On the other hand, the soft particles are deformed in the flow direction at

high shear rates and the microstructural anisotropy is substantially smaller compared to the $g(x,y)$ of the rigid colloids. This is consistent with experimental reports Kalman (2010). Figure 11 shows the pair correlation functions of the suspensions with different moduli, at the highest Péclet numbers of 320 in different planes.

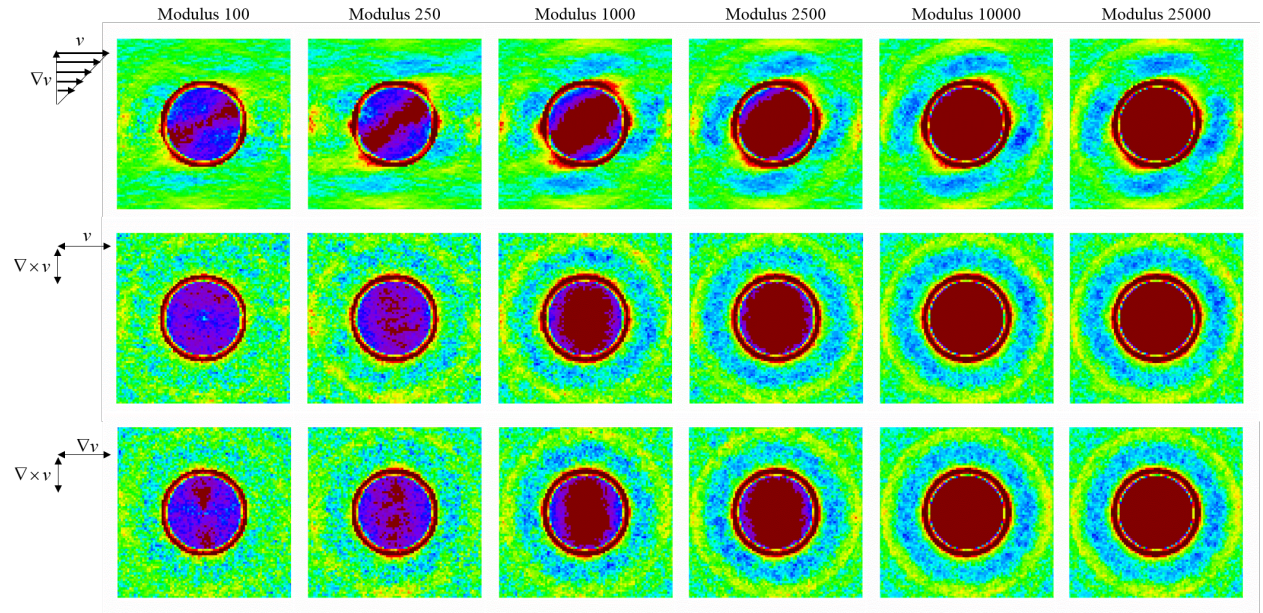


Figure 11. Pair correlation function of the 58% suspensions with different moduli, at $Pe=320$.

The pair correlation function graphs given in figure 11 clearly show the pronounced anisotropy as the colloidal particles become more rigid. Since large and negative second normal stress differences in near hard-sphere suspensions are due to highly anisotropic microstructures that are formed at high shear rates within the hydroclusters (for detailed discussion refer to Foss and Brady (2000)), one can explain the reduced in magnitude and eventually positive N_2 for the soft particles based on the reduced anisotropies observed at high shear rates for particles with lower moduli. One can clearly observe that softer particles are deformed under flow along the compressional axis where the lubrication stresses are high. This in turn suppresses the highly anisotropic structures that are signatures of lubrication forces (top right microstructure in figure

11) and give rise to large (in magnitude) and negative normal stress differences. Additionally, layered structures evident in vorticity planes for the rigid particles are absent for the lower moduli, where particle deformation is the dominant mechanism in defining the microstructure of the suspension.

4. Conclusions

In this work, a comprehensive rheological analysis is reported for a range of soft to rigid suspensions, including measurements of the shear stress, pressure, and normal stress differences is reported for the first time. The corresponding rheological parameters are correlated to the microstructural changes in each suspension by means of pair correlation function graphs. Our simulation model includes along line of centers lubrication hydrodynamics and predicts a continuous and strong shear-thickening behavior at high shear rates for the near hard-sphere suspensions, while suggesting a second shear-thinning regime at very high shear rates for soft suspensions. This is in agreement with experimental measurements of Kalman (2010) for PMMA and Silica particles. The results of our normal stress measurements suggest that the N_1 remains negative and a linearly increasing function of the shear rate at high shear rates, with a slight dependency on the softness/hardness of colloidal particles. N_2 shows a strong dependency on the contact modulus of the solid particles: in the shear-thickening regime N_2 is negative and linearly increases (in magnitude) with shear rate; however, at the onset of second thinning regime for soft particles N_2 begins to decrease in magnitude and eventually reverses its sign at elevated shear rates. This is not observed for near hard-sphere particle suspensions, which only exhibit large and negative N_2 values. Both normal stress differences show strong dependencies on the fraction of colloidal particles. Furthermore, our results show that while at low volume fractions $|N_1| > |N_2|$ for rigid particles, $|N_2|$ grows faster by increasing the colloidal fraction and

eventually in the dense regime it becomes larger than the N_1 . Our study suggests that at high shear rates and for the near hard-sphere suspensions, $P > \sigma > N_2 > N_1$. Using the stress of the suspending fluid at different shear rates, first and second normal stress coefficients, Υ_1 and Υ_2 , and relative viscosity of the suspension, η_r , were defined and for the rigid particles, all three quantities, as well as the pressure of the suspensions found to diverge near the maximum packing fraction. By fitting into empirical models of Eilers and Maron-Pierce we calculated the maximum packing fraction of colloidal particles with different moduli, and correlated it to the rheological response of the suspensions. We showed that the maximum packing fraction decreases at high shear rates as hydroclusters are formed, in agreement with recent experiments [Cwalina and Wagner (2014)]. The maximum packing fraction decreases with increasing particle hardness at high Peclet numbers and the limiting viscosity can be well described by a scaling model for elastohydrodynamics [Kalman (2010)]. The pair correlation functions of the soft suspensions show clear evidence of particle deformation in the flow direction at high shear rates and in the second shear-thinning regime; one can also correlate the positive N_2 elastohydrodynamically-deformed structure formation for soft colloids at high shear rates, where the deformation of particles mitigates the anisotropy generated from the hydrodynamic interactions. As with previous simulations, the use of a simple lubrication hydrodynamics model that neglects tangential interactions provides a semi-quantitative description of experimental observations on model suspensions. Tangential lubrication hydrodynamics and interparticle friction are neglected here in agreement with surface forces measurements of very low coefficients of friction for colloidal particles, however further research is warranted to explore whether they play a role in dilatant behavior, which is not explored here.

Acknowledgments

The authors would like to acknowledge the financial support of the National Science Foundation, NSF, Grant No. CMMI/1068960. This work was supported in part by an allocation of computing time from Ohio Supercomputer Center (OSC) and High Power Computing Center (HPCC) of Case Western Reserve University.

References

- Aral, B. K., and D. M. Kalyon, "Viscoelastic material functions of noncolloidal suspensions with spherical particles," *Journal of Rheology* (1978-present) **41**, 599-620 (1997).
- Ball, R. C., and J. R. Melrose, "Lubrication breakdown in hydrodynamic simulations of concentrated colloids," *Advances in Colloid and Interface Science* **59**, 19-30 (1995).
- Barnes, H. A., "Shear-Thickening ("Dilatancy") in Suspensions of Nonaggregating Solid Particles Dispersed in Newtonian Liquids," *Journal of Rheology* **33**, 329-366 (1989).
- Barroso, E. G., F. M. Duarte, M. Couto, and J. M. Maia, "High strain rate rheological characterization of low viscosity fluids," *Polymer Testing* **29**, 419-424 (2010).
- Bender, J., and N. J. Wagner, "Reversible shear thickening in monodisperse and bidisperse colloidal dispersions," *Journal of Rheology* **40**, 899-916 (1996).
- Bergenholtz, J., J. F. Brady, and M. Vicic, "The non-Newtonian rheology of dilute colloidal suspensions," *Journal of Fluid Mechanics* **456**, 239-275 (2002).
- Brown, E., and H. M. Jaeger, "Shear thickening in concentrated suspensions: phenomenology, mechanisms and relations to jamming," *Reports on Progress in Physics* **77**, 046602 (2014).
- Cheng, X., J. H. McCoy, J. N. Israelachvili, and I. Cohen, "Imaging the Microscopic Structure of Shear Thinning and Thickening Colloidal Suspensions," *Science* **333**, 1276-1279 (2011).
- Cwalina, C. D., and N. J. Wagner, "Material properties of the shear-thickened state in concentrated near hard-sphere colloidal dispersions," *Journal of Rheology* (1978-present) **58**, 949-967 (2014).
- D'Haene, P., J. Mewis, and G. G. Fuller, "Scattering Dichroism Measurements of Flow-Induced Structure of a Shear Thickening Suspension," *Journal of Colloid and Interface Science* **156**, 350-358 (1993).
- de Kruif, C. G., E. M. F. van Iersel, A. Vrij, and W. B. Russel, "Hard sphere colloidal dispersions: Viscosity as a function of shear rate and volume fraction," *The Journal of Chemical Physics* **83**, 4717-4725 (1985).
- Eilers, H., "Die Viskosität von Emulsionen hochviskoser Stoffe als Funktion der Konzentration," *Kolloid-Zeitschrift* **97**, 313-321 (1941).
- Espanol, P., and P. Warren, "Statistical Mechanics of Dissipative Particle Dynamics," *Europhysics Letters* **30**, 191-196 (1995).

- Fernandez, N., R. Mani, D. Rinaldi, D. Kadau, M. Mosquet, H. Lombois-Burger, J. Cayer-Barrioz, H. J. Herrmann, N. D. Spencer, and L. Isa, "Microscopic Mechanism for Shear Thickening of Non-Brownian Suspensions," *Physical Review Letters* **111**, 108301 (2013).
- Foss, D. R., and J. F. Brady, "Structure, diffusion and rheology of Brownian suspensions by Stokesian Dynamics simulation," *Journal of Fluid Mechanics* **407**, 167-200 (2000).
- Ghoufi, A., and P. Malfreyt, "Coarse grained simulations of the electrolytes at the water-air interface from many body Dissipative Particle Dynamics," *Journal of Chemical Theory and Computation* **8**, 787-791 (2012).
- Groot, R. D., and P. B. Warren, "Dissipative particle dynamics: Bridging the gap between atomistic and mesoscopic simulation," *Journal of Chemical Physics* **107**, 4423-4435 (1997).
- Gurnon, A. K., and N. J. Wagner, "Microstructure and rheology relationships for shear thickening colloidal dispersions," *Journal of Fluid Mechanics* **769**, 242-276 (2015).
- Heussinger, C., "Shear thickening in granular suspensions: Interparticle friction and dynamically correlated clusters," *Physical Review E* **88**, 050201 (2013).
- Hoffman, R. L., "Discontinuous and Dilatant Viscosity Behavior in Concentrated Suspensions. I. Observation of a Flow Instability," *Transactions of The Society of Rheology (1957-1977)* **16**, 155-173 (1972).
- Hoogerbrugge, P. J., and J. M. V. A. Koelman, "Simulating Microscopic Hydrodynamic Phenomena with Dissipative Particle Dynamics," *Europhysics Letters* **19**, 155-160 (1992).
- Irving, J. H., and J. G. Kirkwood, "The Statistical Mechanical Theory of Transport Processes. IV. The Equations of Hydrodynamics," *The Journal of Chemical Physics* **18**, 817-829 (1950).
- Jamali, S., M. Yamanoi, and J. Maia, "Bridging the gap between microstructure and macroscopic behavior of monodisperse and bimodal colloidal suspensions," *Soft Matter* **9**, 1506-1515 (2013).
- Kalman, D. P., and N. J. Wagner, "Microstructure of shear-thickening concentrated suspensions determined by flow-USANS," *Rheologica Acta* **48**, 897-908 (2009).
- Kalman, D. P. "Microstructure and rheology of concentrated suspensions of near hard-sphere colloids." Ph.D. thesis, University of Delaware, Newark, DE, 2010.
- Kawasaki, T., A. Ikeda, and L. Berthier, "Thinning or thickening? Multiple rheological regimes in dense suspensions of soft particles," *EPL (Europhysics Letters)* **107**, 28009 (2014).
- Laun, H. M., "Rheological properties of aqueous polymer dispersions," *Die Angewandte Makromolekulare Chemie* **123**, 335-359 (1984).
- Laun, H. M., R. Bung, S. Hess, W. Loose, O. Hess, K. Hahn, E. Hiadicke, R. Hingmann, F. Schmidt, and P. Lindner, "Rheological and small angle neutron scattering investigation of shear-induced particle structures of concentrated polymer dispersions submitted to plane Poiseuille and Couette flow," *Journal of Rheology* **36**, 743-787 (1992).
- Laun, H. M., "Normal stresses in extremely shear thickening polymer dispersions," *Journal of Non-Newtonian Fluid Mechanics* **54**, 87-108 (1994).
- Lee, M., M. Alcoutlabi, J. J. Magda, C. Dibble, M. J. Solomon, X. Shi, and G. B. McKenna, "The effect of the shear-thickening transition of model colloidal spheres on the sign of N1 and on

the radial pressure profile in torsional shear flows," *Journal of Rheology* (1978-present) **50**, 293-311 (2006).

Lee, Y. S., E. D. Wetzel, and N. J. Wagner, "The ballistic impact characteristics of Kevlar woven fabrics impregnated with a colloidal shear thickening fluid," *Journal of Materials Science* **38**, 2825-2833 (2003).

Macosko, C. W. Rheology: principles, measurements, and applications. New York, Wiley.

Maranzano, B. J., and N. J. Wagner, "The effects of particle size on reversible shear thickening of concentrated colloidal dispersions," *The Journal of Chemical Physics* **114**, 10514-10527 (2001).

Mari, R., R. Seto, J. F. Morris, and M. M. Denn, "Shear thickening, frictionless and frictional rheologies in non-Brownian suspensions," *Journal of Rheology* (1978-present) **58**, 1693-1724 (2014).

Maron, S. H., and P. E. Pierce, "Application of ree-eyring generalized flow theory to suspensions of spherical particles," *Journal of Colloid Science* **11**, 80-95 (1956).

Meeker, S. P., R. T. Bonnecaze, and M. Cloitre, "Slip and Flow in Soft Particle Pastes," *Physical Review Letters* **92**, 198302 (2004).

Mewis, J., and N. J. Wagner. Colloid Suspension Rheology. New York, Cambridge University Press.

Morris, J. F., "A review of microstructure in concentrated suspensions and its implications for rheology and bulk flow," *Rheologica Acta* **48**, 909–923 (2009).

Russel, W. B., N. J. Wagner, and J. Mewis, "Divergence in the low shear viscosity for Brownian hard-sphere dispersions: At random close packing or the glass transition?," *Journal of Rheology* **57**, 1555-1567 (2013).

Seto, R., R. Mari, J. F. Morris, and M. M. Denn, "Discontinuous Shear Thickening of Frictional Hard-Sphere Suspensions," *Physical Review Letters* **111**, 218301 (2013).

Silbert, L. E., J. R. Melrose, and R. C. Ball, "The rheology and microstructure of concentrated, aggregated colloids," *Journal of Rheology* (1978-present) **43**, 673-700 (1999).

Wagner, N. J., and J. F. Brady, "Shear Thickening in Colloidal Dispersions," *Physics Today* **62**, 27-32 (2009).

Whittle, M., and E. Dickinson, "On Simulating Colloids by Dissipative Particle Dynamics: Issues and Complications," *Journal of Colloid and Interface Science* **242**, 106-109 (2001).

Whittle, M., and K. P. Travis, "Dynamic Simulations of Colloids by Core-Modified Dissipative Particle Dynamics," *Journal of Chemical Physics* **132**, 124906(124901)-124906(124916) (2010).

Wyart, M., and M. E. Cates, "Discontinuous Shear Thickening without Inertia in Dense Non-Brownian Suspensions," *Physical Review Letters* **112**, 098302 (2014).